Concurrent Improvement in Photogain and Speed of a Metal Oxide Nanowire Photodetector through Enhancing Surface Band Bending via Incorporating a Nanoscale Heterojunction

José Ramón Durán Retamal,[†] Cheng-Ying Chen,[†] Der-Hsien Lien,[†] Michael R. S. Huang,[‡] Chin-An Lin,[†] Chuan-Pu Liu,[‡] and Jr-Hau He*,[†]

[†]Institute of Photonics and Optoelectronics & Department of Electrical Engineering, National Taiwan University, Taipei 10617, Taiwan

[‡]Department of Materials Science and Engineering, National Cheng Kung University, Tainan 701, Taiwan

S *Supporting Information*

ABSTRACT: The surface effect on the photodetection of metal oxide nanostructures acting as a double-edged sword achieves ultrahigh photogain but unavoidably prolongs the response time due to slow oxygen adsorption/desorption processes. In this study, we break the compromise to enhance the UV photogain by 3 orders of magnitude as well as increase the photoresponse speed by 5 times via incorporating open-circuit p−n nanoscale heterojunctions (NHJs) by forming single-crystalline p-NiO nanoparticles on n-ZnO nanowires. This is because the formation of NHJs enhances surface band bending of ZnO nanowires, improving the spatial separation efficiency of photogenerated electrons and holes, and passivates the ZnO surfaces by minimizing the interaction of photocarriers with chemisorbed oxygen molecules. The concept using NHJs explores a new pathway toward ultrafast and supersensitive photodetection.

KEYWORDS: ZnO, nanowire, photodetector, surface band bending, surface effect
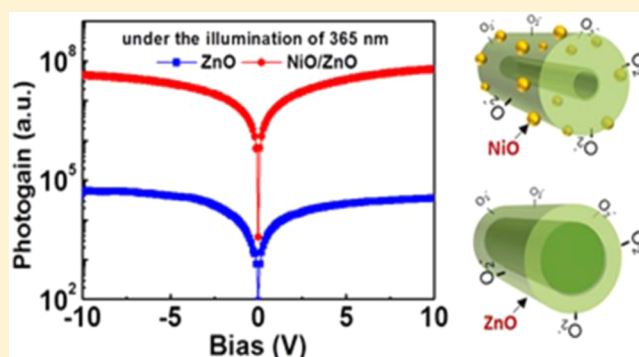
With pronounced surface effects (i.e., oxygen adsorption/desorption) originating from the high surface-to-volume ratio, one-dimensional metal oxide nanostructures exhibit a superior sensitivity to light/chemical molecules, as compared to their thin film counterpart.[1,2] For example, the surface band bending (SBB) (∼1.54 eV) for ZnO nanowires (NWs) arising from the pronounced surface effect could lead to a photogain as high as 10^8 due to the spatial separation of photogenerated electrons and holes in the ZnO NW.[3−5] Much effort has been dedicated to further boost the photoresponse of metal oxide NW photodetectors (PDs). Chen et al. have reported the photoconductive enhancement of ZnO NWs through the localized Schottky junction between the decorated Au nanoparticles (NPs) and the NWs.[6] A low dark-current ultrasensitive ZnO wire PD through piezopotential modulation has been demonstrated, and its physical mechanism is explained by considering both the piezopotential effect and the photon-generated free charge screening effect.[7] Recently the piezo-phototronic effect has also enhanced the performance of optoelectronic devices based on wurtzite materials such as GaN nanobelt (NB) PDs[8] and high-resolution imaging p-GaN/n-ZnO NW array LED pressure/strain sensors.[9] Moreover, it is also of great interest to improve the long response time of ZnO NW PDs caused by the nature of the slow photocarrier

relaxation behavior due to oxygen adsorption/desorption processes.[10] It was reported that using the NB network can significantly improve the relaxation time of nanostructured ZnO PDs due to the existence of the NB−NB junction barriers.[11] Briefly, the surface effects act as a double-edged sword that unavoidably prolongs the response time due to slow oxygen adsorption/desorption processes even though a high photogain is achieved. Several compromise-breaking approaches for enhancing the responsivity as well as reducing the response time have been reported, including an introduction of Schottky junction,[12] polymer surface functionalizations,[13] employment of binary ZnS/ZnO biaxial nanobelts,[14] and the use of metallic core−oxide shell geometry with radial Schottky barriers.[15]

In this study, we demonstrate that p-type single-crystalline NiO NP decoration by Ni deposition and thermal oxidation at 600 °C at the surfaces of n-type ZnO NWs enhances UV photogain of a PD to ∼2.8×10^8, which is 3 orders of magnitude higher than that of pristine ZnO NWs. This is due to the formation of open-circuit p−n nanoscale heterojunctions (NHJs) at the surface of ZnO NWs, which enhances the SBB
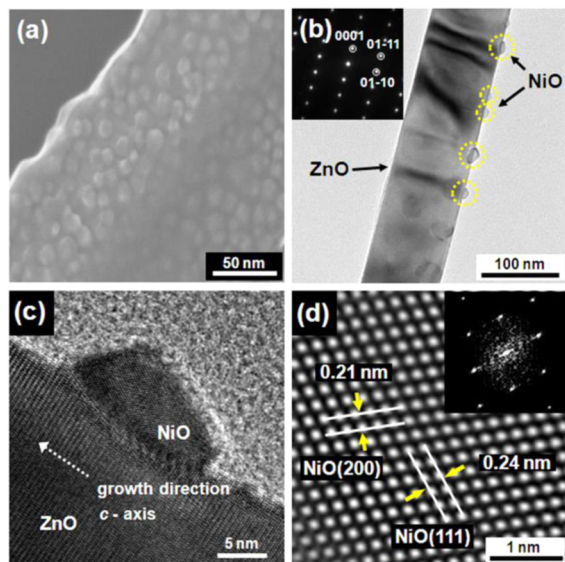
and improves the spatial separation efficiency of photo-generated electrons and holes. The upward band bending can be confirmed by the observation of a threshold gate voltage (V_{th}) shift (from −14.7 V to −6.2 V) from the field-effect transistor (FET) measurement. Moreover, the formation of open-circuit NHJs at ZnO surfaces improves the recovery time of ZnO NWs from 657.4 s to 133.5 s by minimizing the interaction of photocarriers with oxygen molecules through surface passivation. This study demonstrates an effective way to meliorate the performance of nanostructured devices via surface engineering.

■ RESULTS AND DISCUSSION

It has been proven that tailor-made ZnO NWs such as NP-decorated NWs,[6] NB networks,[11] and radial NWs[15] further enhance the UV photodetection properties of pristine ZnO NWs. In this study, p-NiO NPs were decorated on n-ZnO NWs in order to form multiple p−n NHJs that can maximize the functionalized surface, improve the charge transfer, and tune the UV photodetection range. We first synthesized n-ZnO NWs by using a mixture of ZnO:C powders in a furnace at 930 °C. Then, the NWs were decorated with p-NiO NPs synthesized by thermal oxidation of 1-nm-thick Ni thin films in a furnace at 600 °C in an oxygen environment. Finally, the electrode contacts (Ti/Au) were defined by e-beam lithography on SiO₂/Si substrates.

First, the as-fabricated nanostructures were inspected by scanning electron microscopy (SEM) and high-resolution transmission electron microscopy (HRTEM) to study the geometrical and morphological characteristics. Figure 1a shows the SEM image of the NP-decorated ZnO NWs. The coverage ratio of randomly distributed NPs is ∼70% without forming a continuous electrical path along the NW. A TEM image of an NP-decorated NW (Figure 1b) and the corresponding

selective-area electron diffraction pattern (the inset in Figure 1b) indicate that the single-crystalline ZnO NWs are of wurtzite structure and grow along the c-axis.[16] The diameter of the NPs is 10 ± 5 nm, estimated from Figure 1b,c. Furthermore, Figure 1b and c indicate that NPs are single crystalline. The rough ZnO surface after NiO NP formation suggests that the Ni NPs might penetrate the surface of the ZnO NW to form NiO NPs by a thermal oxidation at 600 °C. An HRTEM image of an NP is presented in Figure 1d. According to fast Fourier transformation pattern and measured d-spacing,[17] the NP can be designated as NiO with face-centered-cubic structure.

The current−voltage (I−V) characteristics under dark and 365 nm illumination of the pristine ZnO NW before and after NiO NPs decoration are shown in Figure 2a. Both the pristine
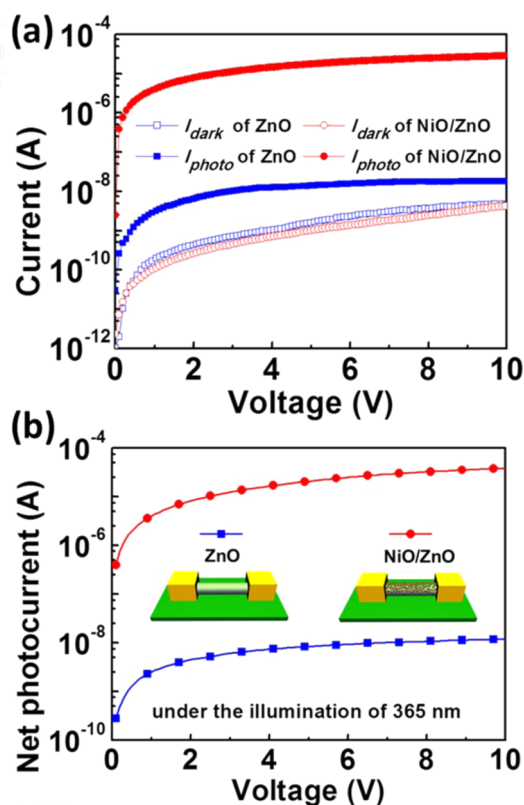
Figure 2. (a) Current−voltage (I−V) characteristics measured in the dark and under 365 nm illumination of 3.14 W/m² at room temperature and (b) net photocurrent−voltage (ΔI−V) characteristics of the ZnO NW before (ZnO) and after NiO NP decoration (NiO/ZnO). (Net photocurrent (ΔI) = photocurrent (I_{photo}) − dark current (I_{dark}).)

ZnO NW and NiO NP-decorated ZnO NW exhibit an increase in current upon exposure to UV light. The net photocurrent−voltage (ΔI−V) characteristics of the pristine ZnO NW and the ZnO NW with NHJs by NiO NP decoration under 365 nm UV illumination are shown in Figure 2b, where the net photo-current (ΔI) is the difference between the photocurrent (I_{photo}) and dark current (I_{dark}). As compared to pristine ZnO NWs, NiO NP-decorated ZnO NWs lead to an impressive photo-current to dark current ratio of 37 100 with an astonishing enhancement factor of 2300 due to the formation of p-NiO/n-ZnO NHJs.

To fairly compare to ZnO with NHJs formed at 600 °C, the pristine ZnO with Ti/Au contacts was annealed at 600 °C for a

Figure 1. (a) SEM image of the NiO NP-decorated ZnO NW. (b) Low-magnification TEM image of a ZnO NW. The dashed circles indicate NiO NPs at the surface, and the inset shows the corresponding electron diffraction pattern of the ZnO NW taken along the [2$\bar{1}\bar{1}$0] zone axis. (c) HRTEM image of the interface between the NiO NPs and ZnO NWs. (d) Magnified HRTEM image of the NiO NP on the ZnO NW surface in (c). The inset in (d) is the corresponding fast Fourier transformation pattern.

very short time before performing the measurements. As shown in the I−V curves depicted in Figure 2a, a slight decrease in the dark current is observed after forming the NiO NPs at the ZnO surfaces by annealing at 600 °C, indicating that the formation of open-circuit NHJs at the surface of ZnO depletes the ZnO. We note that by annealing at 300 °C the electrical properties of Ti/ZnO would be improved due to formation of Ti−O phases and accumulation of oxygen vacancies at the ZnO.[18] However, by annealing at temperatures higher than 500 °C, the contact resistance would increase due to the degradation of the interface and the formation of voids.[19]

Considering the feature size of ZnO NW PDs, the photoresponse can be quantitatively described by the photogain, which is a critical parameter for determining the collection efficiency of photogenerated carriers under illumination. The photogain (G) can be obtained by[5]

$$G = \frac{N_{electron}}{N_{photon}} = \left(\frac{\Delta I}{q}\right)\left(\frac{h\nu}{P}\right)\frac{1}{\eta}$$

(1)

where q is the electron charge, $h\nu$ is the photon energy of incident light, P is the total excitation power absorbed by the NW ($P = I_{ex} \times d \times l$, where I_{ex} is the excitation intensity, l and d are the length and the width of the NW, respectively), and η is the quantum efficiency (for simplicity, $\eta = 1$). As shown in Figure 3a, the photogain spectra of pristine NWs and NWs with NHJs under different bias conditions exhibit a ramp in the UV region due to the remarkable UV absorption of ZnO NWs (band gap ∼3.30 eV) and NiO NPs (band gap ∼3.89 eV). The band gap of NiO NPs was measured and is discussed in the Supporting Information. The photogain is increased with applied bias, and the photogain becomes saturated as the applied bias is increased to 10 V for both pristine NWs and NWs with NHJs, indicating the formation of a saturated depletion of a single NW between two electrodes.[20] The ZnO NW with NHJs shows an ultrahigh photogain peak of ∼2.8 × 10^8 at 330 nm UV illumination and 10 V.

The origin of ultrahigh photogain via forming NHJs by incorporating NiO NPs at the surface of ZnO is stated below. We first start with bare ZnO NWs. As shown in Figure 3b, oxygen molecules acting as electron acceptors tend to chemisorb at the surface by capturing free electrons from pristine ZnO ($O_{2(g)} + e^- \rightarrow O_2^-{}_{(ad)}$), which redistributes the spatial density of the carriers and thus forms the space charge region and the band bending near the surfaces.[3,21] Under UV illumination, photogenerated holes tend to drift to the surface through the electric field built by the surface effect, thereby decreasing the electron−hole recombination possibility. Through oxygen desorption by the neutralization of trapped holes and charged oxygen molecules at the surfaces ($O_2^-{}_{(ad)} + h^+ \rightarrow O_{2(g)}$), the lifetime of the electrons is further prolonged. The electron−hole separation effect induced by the surface electric field explains the high photogain of a single ZnO NW PD. The mechanism of the photocurrent enhancement by open-circuit NHJs via NiO NP decoration can be elucidated as follows. By joining p-type NiO NPs at the surface of n-type ZnO NWs, many open-circuit nanoscale p−n junctions are formed between NiO NPs and ZnO NWs. Since the Fermi energy must be equal in both p-type NiO and n-type ZnO in thermal equilibrium, an electric field forms between the positive ion cores in the n-type ZnO NWs and negative ion cores in p-type NiO NPs, which results in the upward band bending from ZnO to NiO. This NHJ would increase the width and the
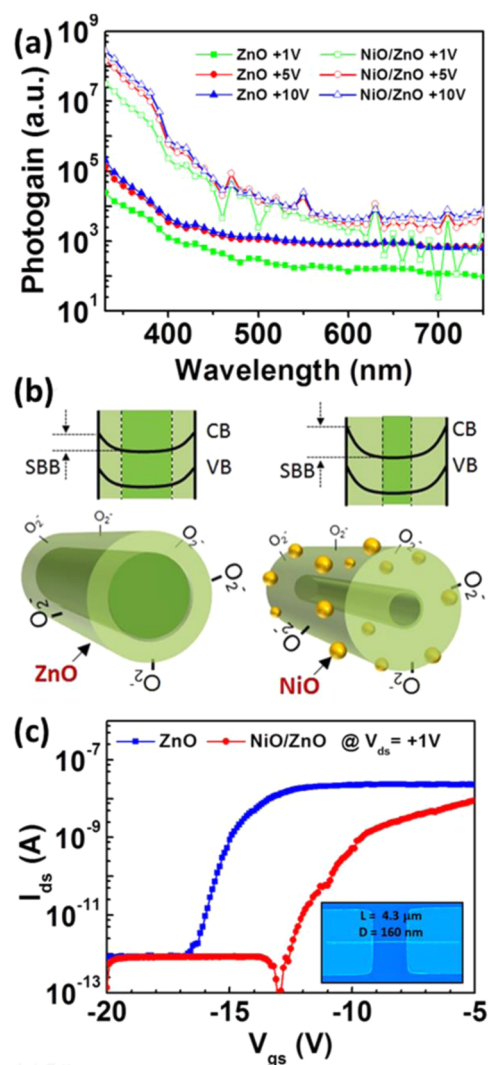
Figure 3. (a) Photogain spectra of pristine ZnO NWs and ZnO NWs with NHJs at biases of 1, 5, and 10 V. (b) Schematics of the SBB caused by oxygen chemisorption for pristine NWs and NWs with NHJs. (c) FET transfer characteristics of the pristine ZnO NWs and the ZnO NWs with NHJs at V_{ds} = 1 V. The inset in (c) is a SEM image of the ZnO NW FET with a diameter of 160 nm and an active length of 4.3 μm.

height of the SBB region, which would facilitate photogenerated carrier sweeping in the ZnO NWs. As compared with the pristine ZnO NW PDs, the spatial electron−hole separation effect is pronounced and the recombination rate of electrons and holes under UV illumination is further reduced for a NiO NP-decorated ZnO NW PD, giving rise to a prolonged electron lifetime. Accordingly, the remaining photogenerated electrons in the NW core contribute to the increase of the photocurrent. Moreover, we note that it is difficult to estimate the actual surface electric field of ZnO NWs after incorporating NiO NPs since the charge distribution for p-type NPs at the nanoscale might be different from that of a typical semiconductor model. A quantitative understanding of the NHJ will be needed to further increase the device efficiencies and functionalities for facilitating broad applications in NW-based electronics and optoelectronics.

Since ZnO is naturally an n-type wide-band-gap semiconductor, growing stable and reproducible p-type ZnO is

difficult. Regardless of difficulty, stability, and reproducibility, UV photodiodes based on a p-$Mg_{0.2}Zn_{0.8}O$/n-ZnO junction have been achieved with a considerable wide response range but low responsivity (~10^{-4} A/W) caused by a high density of defects.[22] As an alternative to p-type ZnO, a variety of p-type materials have been combined with ZnO to form p−n heterojunctions. p-Si,[23] p-Cu_2O,[24] p-CdTe,[25] and p-HgTe[26] with a narrow band gap would block the UV absorption of ZnO, sacrificing visible-blind photodetection characteristics of ZnO. Moreover, p-6H-SiC,[27] p-4H-SiC,[28] and p-GaN[29] have similar wurtzite crystal structures, low lattice mismatch to ZnO (4%, 5%, and 1.8%, respectively), wide band gap (2.9 eV, 3.2, and 3.4 eV, respectively), and type-II energy band alignment with n-ZnO. However, conduction and valence band offset between ZnO and these p-type materials are low, theoretically leading to thinner space charge regions with lower SBB. Alternatively, NiO is a p-type semiconductor with a wider band gap of 3.7 eV and low lattice mismatch with ZnO (~9%) and forms a type-II energy band alignment with large conduction and valence band offset with n-ZnO.[30] Altogether this makes p-NiO a perfect candidate to functionalize the n-ZnO surface by forming NHJs to enhance the SBB of ZnO NWs for high photogain and improved photoresponse.

As shown in Figure 3c, we also have measured the drain current−gate voltage (I_{ds}−V_{gs}) characteristics of the ZnO NW with and without NiO NPs to have a direct comparison of the FET characteristics with the SBB model proposed in Figure 3b. The I_{ds}−V_{gs} curves yield threshold voltages (V_{th}) of −14.7 and −6.2 V for the pristine NW and the NiO NP-decorated ZnO NW, respectively, indicating the ZnO NW FET under the different surface conditions is always in normal on-type depletion-mode. Note that the V_{th} is defined as the gate voltage obtained by extrapolating the linear portion of the I_{ds}−V_{gs} characteristics from the point of maximum slope to zero drain current, in which the point of maximum slope is the point where the transconductance (g_m = dI_{ds}/dV_{gs}) is maximal. This result also suggests that the FET property, e.g., V_{th}, is tunable through modulation of surface effects. Additionally, assuming that the NW is a cylinder on an infinite metal plate,[21] the carrier concentration (n_e) of the NW can be obtained by

$$n_e = |V_{gs} - V_{th}|C_g / q\pi r^2 L \qquad (2)$$

where the capacitance (C_g) per unit length is $2\pi\varepsilon_0\varepsilon_{(SiO2)}L/\cosh^{-1}((h + r)/r)$ (where ε_{SiO2} is the dielectric constant of the SiO_2 (3.9), ε_0 is the permittivity of free space, and h is the oxide layer thickness), r is the NW radius, and L is the channel length. The results indicate that the carrier concentration after the formation of NHJs is decreased from 6.83×10^{17} cm^{-3} to 2.88×10^{17} cm^{-3} at V_{gs} = 0 V, implying that NiO NP-decorated ZnO NWs have a tight open conducting channel, which is consistent with the SBB model proposed in Figure 3b.

The time-resolved photocurrent measurements were performed by switching on and off the 365 nm illumination of 3.14 W/m², as shown in Figure 4a. The photocurrents of both pristine and NiO NP-decorated NWs are rapidly elevated and gradually saturated under steady illumination and then slowly descend as the illumination is switched off. It is known that the fast photocurrent rise after turning on the UV light results from rapid photogenerated carriers, and the slow photocurrent decay after switching the UV light off is governed by the slow surface-related process, i.e., the slow rechemisorption rate of oxygen molecules ($O_{2(g)}$ + e^- → $O_2^-_{(ad)}$).[3,31,32] To quantify the
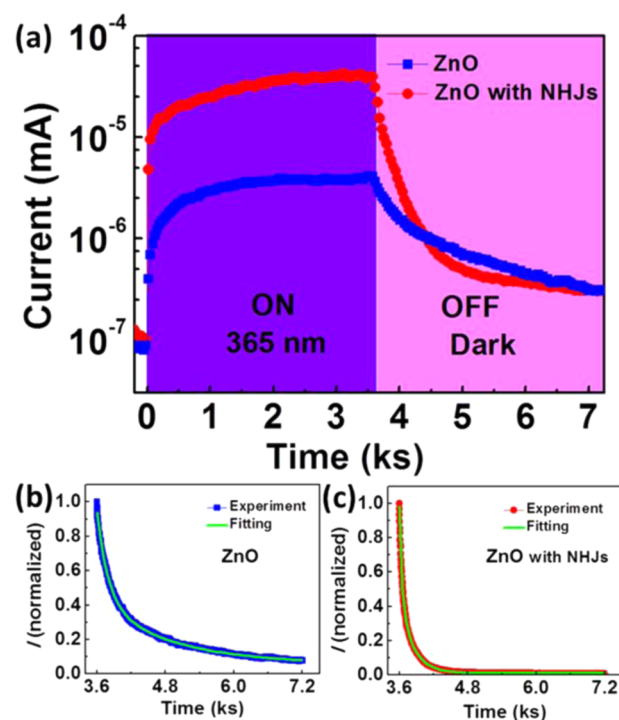
Figure 4. (a) Time-resolved photocurrents of the pristine ZnO NW and the ZnO NW with NHJs at a bias of 1 V under the 365 nm illumination of 3.14 W/m². Experimental curves (blue and red) and fitted curves (green) for the recovery behavior of the normalized currents: (b) pristine ZnO NW and (c) ZnO NW with NHJs.

photocurrent decay, the normalized relaxation dynamics of pristine and NiO NP-decorated NW PDs is fitted by second-order exponential decay functions, $I = I_0 + A_1 e^{(t/\tau 1)} + A_2 e^{(t/\tau 2)}$, where I_0 is the ultimate dark current after the photorelaxation process, A_1 and A_2 are weighing factors that quantify the relative contribution of each mechanism, and τ_1 and τ_2 are time constants. By choosing, $\tau_1 < \tau_2$, τ_1 (τ_2) is the shorter (longer) time constant corresponding to the faster (slower) process, which is ascribed to a bulk (surface) dominated process. Therefore, $1/\tau_2$ and $1/\tau_1$ are related to the surface oxygen readsorption rate and the bulk recombination rate. It should be noted that both processes occur at the same time. The fitting results are depicted in Figure 4b and c, respectively. In the analysis, t = 0 was set as the time the illumination is switched off. Note that the photocurrent reaches a steady state under the 365 nm illumination before switching off. The photorelaxation time constants (τ_1 = 197.4 s and τ_2 = 1319.4 s) for the pristine NW can be extracted with relative weight factors of 59% and 41%, respectively, while the two photorelaxation time constants for the NiO NP-decorated NW are τ_1 = 47.2 s and τ_2 = 234.9 s with relative weight factors of 54% and 46%, respectively. An effective recovery time ($\tau_{eff} = A_1\tau_1 + A_2\tau_2$) of 133.5 s for the NiO NP-decorated NW is nearly 5 times shorter than that of the pristine one (657.4 s). The results reveal that the formation of NHJs at ZnO surfaces by employing NiO NPs improves the relaxation dynamics of ZnO NW by minimizing the interaction of photocarriers with oxygen molecules due to surface passivation.[25,33,34]

■ **CONCLUSION**

In summary, we demonstrated that the decoration of p-type NiO NPs on n-type ZnO NWs can greatly improve the

photogain in the UV regions. The improved photogain is up to ~2.8×10^8, which is 3 orders of magnitude higher than that of the pristine ZnO NWs. The underlying mechanism is ascribed to the formation of p–n NHJs at the surface of ZnO NWs with a coverage ratio of ~70%, which enhances the spatial separation efficiency of photogenerated electrons and holes by increasing the width and height of the SBB region. Enhanced SBB via incorporating NHJs is confirmed by the observation of a V_{th} shift (from −14.7 V to −6.2 V) of ZnO NW FETs after NiO NP decoration at the surface of ZnO NWs. Furthermore, the formation of NiO NPs at the ZnO surface improves the recovery time of the ZnO NW from 657.4 s to 133.5 s by minimizing the interaction of photocarriers with oxygen molecules via surface passivation. Our study provides the strategies for optimizing the performance of NW-based optical devices through surface engineering.

■ METHODS

ZnO NWs were prepared by heating the mixed ZnO and C powders (6.6 g:3.3 g) in a furnace at 930 °C for 1 h using the vapor–liquid–solid method.[35] Si substrates with 2-nm-thick Au as the metal catalyst were placed 5–10 cm near the source. NWs were then transferred to insulating SiO_2/Si substrates. NWs were adhered to the substrate by van der Waals force. For device fabrication, Ti/Au (60/40 nm) electrodes were patterned by an e-beam lithography process and deposited by an electron gun evaporator. For the formation of the p-NiO NPs, 1-nm-thick Ni was deposited by electron gun evaporation and further oxidized by annealing at 600 °C with 200 sccm O_2 (99.99%) and 100 sccm N_2 (99.99%) flows.[36] Microstructure analysis of the as-synthesized NiO NP-decorated ZnO NW was carried out with SEM (JEOL JSM-6700F) and HRTEM (JEOL 2100F with Cs corrector). The photoconduction characteristics were examined with a Keithley 4200 SC semiconductor parameter analyzer in the air at room temperature. The illumination source was a halogen lamp coupled to an SP CM110 monochromator.

■ ASSOCIATED CONTENT

ⓢ Supporting Information

The measurement of the band gap of NiO NPs by extrapolation of the linear region of the dependence of $(\alpha h\nu)^2$ on the incident photon energy $(h\nu)$. This information is available free of charge via the Internet at http://pubs.acs.org.

■ AUTHOR INFORMATION

Corresponding Author
*E-mail: jhhe@cc.ee.ntu.edu.tw.

Notes
The authors declare no competing financial interest.

■ ACKNOWLEDGMENTS

■ REFERENCES

(1) Zhai, T.; Fang, X.; Liao, M.; Xu, X.; Zeng, H.; Yoshio, B.; Golberg, D. A Comprehensive Review of One-Dimensional Metal-Oxide Nanostructure Photodetectors. *Sensors* **2009**, *9*, 6504–6529.

(2) Soci, C.; Zhang, A.; Bao, X. Y.; Kim, H.; Lo, Y.; Wang, D. Nanowire Photodetectors. *J. Nanosci. Nanotechnol.* **2010**, *10*, 1430–1449.

(3) Chen, C. Y.; Durán Retamal, J. R.; Wu, I. W.; Lien, D. H.; Chen, M. W.; Ding, Y.; Chueh, Y. L.; Wu, C. I.; He, J. H. Probing Surface Band Bending of Surface-Engineered Metal Oxide Nanowires. *ACS Nano* **2012**, *6*, 9366–9372.

(4) He, J. H.; Chang, P. H.; Chen, C. Y.; Tsai, K. T. Electrical and Optoelectronic Characterization of a ZnO Nanowire Contacted by Focused-Ion-Beam-Deposited Pt. *Nanotechnology* **2009**, *20*, 135701–135705.

(5) Soci, C.; Zhang, A.; Xiang, B.; Dayeh, S. A.; Aplin, D. P. R.; Park, J.; Bao, X. Y.; Lo, Y. H.; Wang, D. ZnO Nanowire UV Photodetectors with High Internal Gain. *Nano Lett.* **2007**, *7*, 1003–1009.

(6) Chen, M. W.; Chen, C. Y.; Lien, D. H.; Ding, Y.; He, J. H. Photoconductive Enhancement of Single ZnO Nnanowire through Localized Schottky Effects. *Opt. Express* **2010**, *18*, 14836–14841.

(7) Yang, Q.; Guo, X.; Wang, W.; Zhang, Y.; Xu, S.; Lien, D. H.; Wang, Z. L. Enhancing Sensitivity of a Single ZnO Micro-/Nanowire Photodetector by Piezo-phototronic Effect. *ACS Nano* **2010**, *4*, 6285–6291.

(8) Yu, R.; Pan, C.; Hu, Y.; Li, L.; Liu, H.; Liu, W.; Chua, S.; Chi, D.; Wang, Z. Enhanced Performance of GaN Nanobelt-Based Photodetectors by Means of Piezotronic Effects. *Nano Res.* **2013**, *6*, 758–766.

(9) Pan, C.; Dong, L.; Zhu, G.; Niu, S.; Yu, R.; Yang, Q.; Liu, Y.; Wang, Z. L. High-Resolution Electroluminescent Imaging of Pressure Distribution Using a Piezoelectric Nanowire LED Array. *Nat. Photonics* **2013**, *7*, 752–758.

(10) Chen, M. C.; Durán Retamal, J. R.; Chen, C. Y.; He, J. H. Photocarrier Relaxation Behavior of a Single ZnO Nanowire UV Photodetector: Effect of Surface Band Bending. *IEEE Electron Device Lett.* **2012**, *33*, 411–413.

(11) Chen, C. Y.; Chen, M. W.; Hsu, C. Y.; Lien, D. H.; Chen, M. J.; He, J. H. Enhanced Recovery Speed of Nanostructured ZnO Photodetectors Using Nanobelt Networks. *IEEE J. Sel. Top. Quantum Electron.* **2012**, *18*, 1807–1811.

(12) Zhou, J.; Gu, Y.; Hu, Y.; Mai, W.; Yeh, P. H.; Bao, G.; Sood, A. K.; Polla, D. L.; Wang, Z. L. Gigantic Enhancement in Response and Reset Time of ZnO UV Nanosensor by Utilizing Schottky Contact and Surface Functionalization. *Appl. Phys. Lett.* **2009**, *94*, 191103–191103.

(13) Lao, C. S.; Park, M. C.; Kuang, Q.; Deng, Y.; Sood, A. K.; Polla, D. L.; Wang, Z. L. Giant Enhancement in UV Response of ZnO Nanobelts by Polymer Surface-Functionalization. *J. Am. Chem. Soc.* **2007**, *129*, 12096–12097.

(14) Hu, L.; Yan, J.; Liao, M.; Xiang, H.; Gong, X.; Zhang, L.; Fang, X. An Optimized Ultraviolet-A Light Photodetector with Wide-Range Photoresponse Based on ZnS/ZnO Biaxial Nanobelt. *Adv. Mater.* **2012**, *24*, 2305–2309.

(15) Hsu, C. Y.; Lien, D. H.; Lu, S. Y.; Chen, C. Y.; Kang, C. F.; Chueh, Y. L.; Hsu, W. K.; He, J. H. Supersensitive, Ultrafast, and Broad-Band Light-Harvesting Scheme Employing Carbon Nanotube/TiO_2 Core–Shell Nanowire Geometry. *ACS Nano* **2012**, *6*, 6687–6692.

(16) He, J. H.; Ho, C. H.; Wang, C. W.; Ding, Y.; Chen, L. J.; Wang, Z. L. Growth of Crossed ZnO Nanorod Networks Induced by Polar Substrate Surface. *Cryst. Growth Des.* **2008**, *9*, 17–19.

(17) Hotovy, I.; Huran, J.; Spiess, L. Characterization of Sputtered NiO Films Using XRD and AFM. *J. Mater. Sci.* **2004**, *39*, 2609–2612.

(18) Brillson, L. J.; Lu, Y. ZnO Schottky Barriers and Ohmic Contacts. *J. Appl. Phys.* **2011**, *109*, 121301.

(19) Kim, H. K.; Han, S. H.; Seong, T. Y.; Choi, W. K. Low-Resistance Ti/Au Ohmic Contacts to Al-Doped ZnO Layers. *Appl. Phys. Lett.* **2000**, *77*, 1647.

(20) Tsai, D. S.; Liu, K. K.; Lien, D. H.; Tsai, M. L.; Kang, C. F.; Lin, C. A.; Li, L. J.; He, J. H. Few-Layer MoS_2 with High Broadband Photogain and Fast Optical Switching for Use in Harsh Environments. *ACS Nano* **2013**, *7*, 3905–3911.

(21) Chen, C. Y.; Chen, M. W.; Ke, J. J.; Lin, C. A.; Durán Retamal, J. R.; He, J. H. Surface Effects on Optical and Electrical Properties of ZnO Nanostructures. *Pure Appl. Chem.* **2010**, *82*, 2055–2073.

(22) Li, Y. F.; Yao, B.; Deng, R.; Li, B. H.; Zhang, J. Y.; Zhao, Y. M.; Jiang, D. Y.; Zhang, Z. Z.; Shan, C. X.; Shen, D. Z.; Fan, X. W.; Lu, Y. M. Ultraviolet Photodiode Based on p-$Mg_{0.2}Zn_{0.8}$O/n-ZnO Heterojunction with Wide Response Range. *J. Phys. D: Appl. Phys.* **2009**, *42*, 105102.

(23) Huang, C. Y.; Yang, Y. J.; Chen, J. Y.; Wang, C. H.; Chen, Y. F.; Hong, L. S.; Liu, C. S.; Wu, C. Y. p-Si Nanowires/SiO_2/n-ZnO Heterojunction Photodiodes. *Appl. Phys. Lett.* **2010**, *97*, 013503.

(24) Wang, R. C.; Lin, H. Y. Simple Fabrication and Improved Photoresponse of ZnO-Cu_2O Core-Shell Heterojunction Nanorod Arrays. *Sens. Actuators, B* **2010**, *149*, 94−97.

(25) Aga, J. R. S.; Jowhar, D.; Ueda, A.; Pan, Z.; Collins, W. E.; Mu, R.; Singer, K. D.; Shen, J. Enhanced Photoresponse in ZnO Nanowires Decorated with CdTe Quantum Dot. *Appl. Phys. Lett.* **2007**, *91*, 232108.

(26) Seong, H.; Kyoungah, C.; Sangsig, K. A pn Heterojunction Diode Constructed with n-Type ZnO Nanowire and a p-Type HgTe Nanoparticle Thin Film. *Appl. Phys. Lett.* **2009**, *94*, 043102.

(27) Alivov, Y. I.; Ozgur, U.; Dogan, S.; Johnstone, D.; Avrutin, V.; Onojima, N.; Liu, C.; Xie, J.; Fan, Q.; Morkoc, H. Photoresponse of n-ZnO/p-SiC Heterojunction Diodes Grown by Plasma-Assisted Molecular-Beam Epitaxy. *Appl. Phys. Lett.* **2005**, *86*, 241108.

(28) Lee, J. S.; Kim, S. C.; Moon, B. M.; Wook, B.; Kim, S. C.; Kim, N. K.; Koo, S. M. In Epitaxial ZnO/4H-SiC Heterojunction Diodes. *Int. Nanoelectron. Conf., 3rd* **2010**, 706−707.

(29) Chen, C. H.; Chang, S. J.; Chang, S P.; Li, M. J.; Chen, I. C.; Hsueh, T. J.; Hsu, C. L. Novel Fabrication of UV Photodetector Based on ZnO Nanowire/p-GaN Heterojunction. *Chem. Phys. Lett.* **2009**, *476*, 69−72.

(30) Deng, R.; Yao, B.; Li, Y. F.; Zhao, Y. M.; Li, B. H.; Shan, C. X.; Zhang, Z. Z.; Zhao, D. X.; Zhang, J. Y.; Shen, D. Z.; Fan, X. W. X-ray Photoelectron Spectroscopy Measurement of n-ZnO/p-NiO Heterostructure Valence-Band Offset. *Appl. Phys. Lett.* **2009**, *94*, 022108.

(31) Li, Q. H.; Gao, T.; Wang, Y. G.; Wang, T. H. Adsorption and Desorption of Oxygen Probed from ZnO Nanowire Films by Photocurrent Measurements. *Appl. Phys. Lett.* **2005**, *86*, 123117−123119.

(32) Zhang, D. H. Adsorption and Photodesorption of Oxygen on the Surface and Crystallite Interfaces of Sputtered ZnO Films. *Mater. Chem. Phys.* **1996**, *45*, 248−252.

(33) Chen, C. Y.; Lin, C. A.; Chen, M. J.; Lin, G. R.; He, J. H. ZnO/Al_2O_3 Core−Shell Nanorod Arrays: Growth, Structural Characterization, and Luminescent Properties. *Nanotechnology* **2009**, *20*, 185605−185609.

(34) Moazzami, K.; Murphy, T. E.; Phillips, J. D.; Cheung, M. C. K.; Cartwright, A. N. Sub-bandgap Photoconductivity in ZnO Epilayers and Extraction of Trap Density Spectra. *Semicond. Sci. Technol.* **2006**, *21*, 717−723.

(35) Ramgir, N. S.; Subannajui, K.; Yang, Y.; Grimm, R.; Michiels, R.; Zacharias, M. Reactive VLS and the Reversible Switching between VS and VLS Growth Modes for ZnO Nanowire Growth. *J. Phys. Chem. C* **2010**, *114*, 10323−10329.

(36) Auret, F. D.; Wu, L.; Meyer, W. E.; Nel, J. M.; Legodi, M. J.; Hayes, M. Electrical Characterisation of NiO/ZnO Structures. *Phys. Status Solidi C* **2004**, *1*, 674−677.